NANO LETTERS

Letter

pubs.acs.org/NanoLett

Effective Cleaning of Hexagonal Boron Nitride for Graphene Devices

Andrei G. F. Garcia,*[,†] Michael Neumann,[‡] François Amet,[‡] James R. Williams,[‡] Kenji Watanabe,[§] Takashi Taniguchi,[§] and David Goldhaber-Gordon*[,‡]

[†]Department of Applied Physics and [‡]Department of Physics, McCullough Building, Stanford University, Stanford, California 94305-4045, United States

[§]National Institute for Materials Science, 1-1 Namiki, Tsukuba, 305-0044, Japan

Supporting Information

做石墨烯衬底

ABSTRACT: Hexagonal boron nitride (h-BN) films have attracted considerable interest as substrates for graphene. (Dean, C. R. et al. *Nat. Nanotechnol.* **2010**, *5*, 722−6; Wang, H. et al. *Electron Device Lett.* **2011**, *32*, 1209−1211; Sanchez-Yamagishi, J. et al. *Phys. Rev. Lett.* **2012**, *108*, 1−5.) We study the presence of organic contaminants introduced by standard lithography and substrate transfer processing on h-BN films exfoliated on silicon oxide substrates. Exposure to photoresist processing adds a large broad luminescence peak to the Raman spectrum of the h-BN flake. This signal persists through typical furnace annealing recipes (Ar/H_2). A recipe that successfully removes organic contaminants and results in clean h-BN flakes involves treatment in Ar/O_2 at 500 °C.

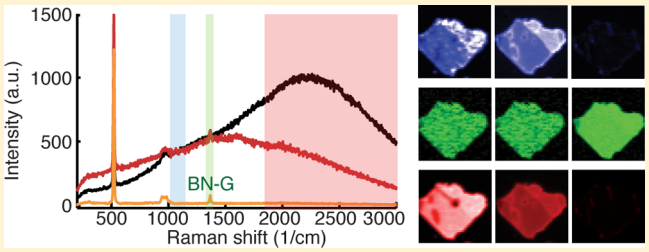

KEYWORDS: *Boron nitride, Raman, organic residue removal, graphene*

Recently, hexagonal boron nitride (h-BN) has been used extensively as a substrate for electronic studies on graphene.[1−5] When graphene is exfoliated directly onto silicon oxide (SiO_2), the carrier mean free path is limited by scattering off charged impurities inside the substrate[6,7] and by the surface roughness of amorphous SiO_2.[8,9] This problem can be resolved by interposing a thin layer of h-BN between SiO_2 and graphene. The insulating h-BN separates the graphene from charged impurities and provides a smoother substrate, increasing the mean free path to hundreds of nanometers and opening up the possibility of ballistic devices.[10] The ease of exfoliating h-BN adds to its suitability as a substrate.

For h-BN to perform the function described above, substrate cleanliness is critical. In this article, we present the first systematic study of the presence and influence of organic contaminants introduced onto h-BN substrates by standard lithographic processing steps required to fabricate complex sample structures, and we introduce a recipe for the successful removal of such contaminants.

In this work, we use confocal Raman microscopy and intermittent-contact mode atomic force microscopy (AFM) to study h-BN flakes deposited onto oxidized silicon substrates. To illustrate the signature of organic contaminants, Figure 1 shows the Raman spectrum of a h-BN flake that underwent the standard processing steps of exfoliation using adhesive tape, spin-coating with photoresist and photoresist removal using organic solvents (acetone and isopropyl alcohol (IPA)). The Raman spectrum of the flake (black line) includes the G-band of h-BN (green line) and the spectral features of the thermally oxidized silicon substrate (brown line). However, the flake's Raman response is dominated by a broad excess spectrum that reflects the presence of organic processing residues. Empirically, we find that the excess spectrum can be described by a superposition of three Gaussian line shapes[11] (see figure caption for details) that we assign to adhesive residue from the exfoliation process (blue line) and photoresist (red and purple lines).

A recipe that is frequently used in an attempt to remove residues of adhesive stemming from exfoliation and photoresist from graphene and h-BN flakes is a heat treatment at 300−350 °C in an Ar/H_2 atmosphere.[1] We find that this recipe is ineffective at removing adhesive residue (Figure 2) and/or photoresist (Figure 3) from h-BN, as are subsequent heat treatments in Ar/H_2 atmosphere at 500 °C.

In the case of adhesive residue, the AFM topography image acquired after heat treatment in Ar/H_2 atmosphere (Figure 2a) exhibits prominent surface features. After an initial treatment at 350 °C, Raman spectra of the h-BN flake (shown for locations with and without prominent topographical features in Figure 2b,c, respectively) exhibit a significant reduction of the broad excess spectrum that dominated the Raman response prior to heat treatment. However, a subsequent treatment at the higher temperature of 500 °C recovers a broad excess spectrum. This effect is reflected in Raman maps obtained by integrating over a spectral range that is dominated by the excess spectrum and in which bulk h-BN and SiO_2 have no Raman peaks (Figure 2d−f).

Received: March 27, 2012
Revised: July 26, 2012
Published: August 6, 2012

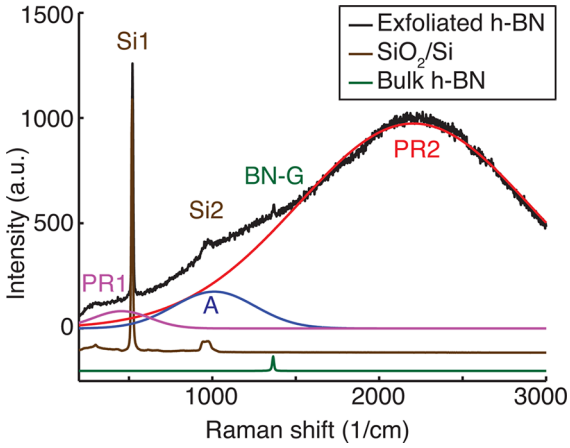

Figure 1. Measured Raman spectrum (black line) of a h-BN flake deposited onto a SiO_2 substrate after standard processing steps: exfoliation using adhesive tape, spin-coating with photoresist, and resist removal with acetone and IPA. The sample has not been heat treated. Flake thickness determined by AFM is 12 nm. Measured spectra of bulk h-BN (green line, BN-G) and a thermally oxidized SiO_2 substrate (brown line, Si1 and Si2) are shown for comparison (offset for clarity). The excess spectral features that dominate the Raman response of the exfoliated h-BN flake are associated with organic contaminants, namely residues of adhesive and photoresist. Empirically, they can be described by a superposition of three Gaussian fits (PR1 - magenta, μ = 440 cm^{-1} and σ = 170 cm^{-1}; A - blue, μ = 1075 cm^{-1} and σ = 500 cm^{-1}; PR2 - red, μ = 2300 cm^{-1} and σ = 450 cm^{-1}).

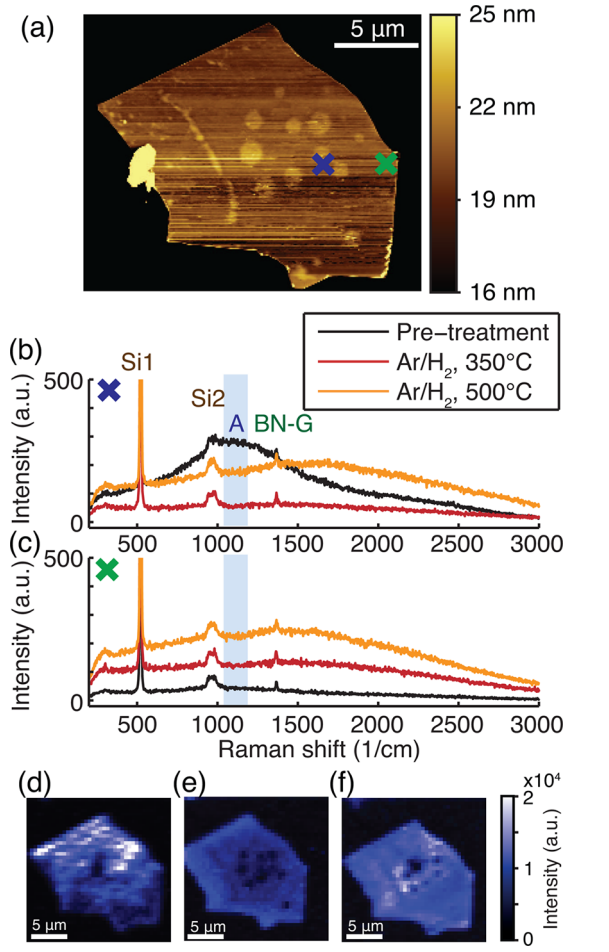

Figure 2. Effect of heat treatment in Ar/H_2 atmosphere in the presence of adhesive residue. (a) AFM topography of h-BN flake exfoliated on SiO_2 after annealing in Ar/H_2. During heat treatment, adhesive residue present on the flake forms prominent topographical features. The evolution of Raman spectra with heat treatment steps at 350 and 500 °C is shown for locations (b) with a large amount of adhesive residue (blue cross), and (c) no visible topographical feature stemming from adhesive (green cross). Spectral intensity maps obtained by integrating over region A that is dominated by the spectral response due to adhesive residue (shaded in blue) are shown (d) before heat treatment, (e) after treatment in Ar/H_2 at 350 °C, (f) after treatment in Ar/H_2 at 500 °C.

These observations provide clear evidence that while heat treatment in Ar/H_2 atmosphere at 350 °C suppresses Raman features associated with the adhesive residue, the organic contaminants remain present on the sample, and heat treatment at 500 °C reinstates an excess Raman spectrum. Features in the Raman maps correlate well with the topographical features in the AFM image. The puddle-like shape of these features suggests that at high temperatures, adhesive residue coalesces due to surface tension effects.

The phenomena seen when residue of photoresist from standard lithographic processing is present on the sample are similar. The AFM topography of a h-BN flake that has undergone photoresist spinning and resist removal in organic solvent (Figure 3a) exhibits puddle-shaped features that clearly indicate the presence of contaminants. A heat treatment in Ar/H_2 at 350 °C will slightly alter the appearance of Raman spectra in areas both with and without prominent topographical features (Figure 3b,c, respectively), but a subsequent treatment at 500 °C leads to a strongly enhanced excess spectrum. Spectral intensity maps obtained by integrating over the excess spectrum (Figure 3d–f) show a strong correlation with features visible in the AFM topography.

In addition, the high-temperature treatment step introduces two new spectral features centered around 1350 and 1600 cm^{-1}, which we identify as the D- and G-bands of amorphous graphitic material,[12,13] indicating that photoresist residue has undergone partial graphitization. From Figure 3b,c, the onset temperature of the graphitization lies between 350 and 500 °C. Integrating over the spectral region occupied by the graphitic G-band (shaded in yellow) leads to a spatial map of graphitic material that strongly resembles the distribution of photoresist (shaded in red) prior to the final heat treatment at 500 °C.

In contrast to the processes involving Ar/H_2 described above, we have found heat treatment at 500 °C in Ar/O_2 atmosphere to be highly effective at removing both adhesive residue (Figure 4) and photoresist (Figure 5) from h-BN flakes. Figure 4a shows the AFM topography of a h-BN flake after heat treatment at 500 °C in Ar/O_2 atmosphere. This flake had been exposed to adhesive during exfoliation, yet very few surface features suggestive of organic residue remain after the Ar/O_2 treatment. The evolution of Raman spectra with treatment at successively higher temperature is shown in Figure 4b,c, corresponding respectively to positions on the sample with and without a prominent excess spectrum initially present. Treatment at 350 °C leads to an enhanced spectrum with broad excess contribution qualitatively similar to those seen for Ar/H_2 treatments at this temperature. In contrast, heat treatment in Ar/O_2 at 500 °C completely eliminates all excess contributions to the Raman spectrum, such that only the spectrum of silicon and the G-band of h-BN are visible, providing clear evidence that all adhesive residue has been removed. Spectral maps (Figure 4d–f) illustrate that this evolution takes place across the entire h-BN flake.

dx.doi.org/10.1021/nl3011726 | Nano Lett. 2012, 12, 4449–4454

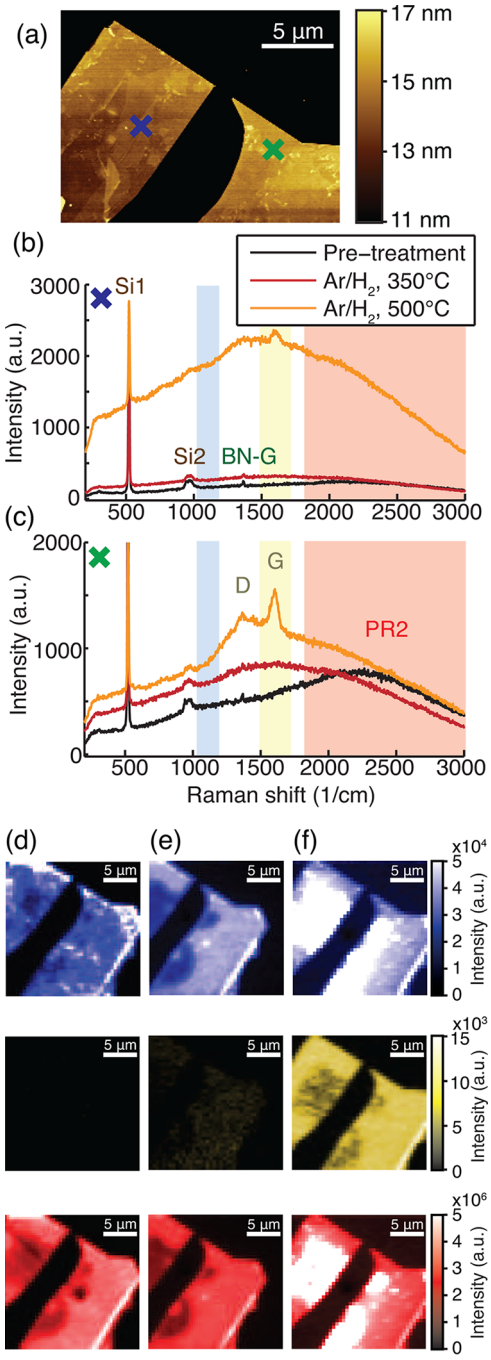

Figure 3. Effect of heat treatment in Ar/H_2 atmosphere in the presence of photoresist residue. (a) AFM topography of h-BN flakes on a SiO_2 substrate, after spin-coating with photoresist, resist removal with acetone and IPA, and subsequent heat treatment. Raman spectra acquired at locations (b) with prominent topographical features due to photoresist residue (blue cross) and (c) without such features (green cross) show a strong evolution with heat treatment. Maps of the sample's Raman response (d) prior to heat treatment, (e) after treatment in Ar/H_2 at 350 °C, and (f) after subsequent heat treatment in Ar/H_2 at 500 °C are obtained by integrating over the spectral range dominated by the broad excess spectrum associated with organic residue (region PR2, shaded in red), and over the range occupied by the emergent graphitic G-band peak of baked organic material (shaded in yellow).

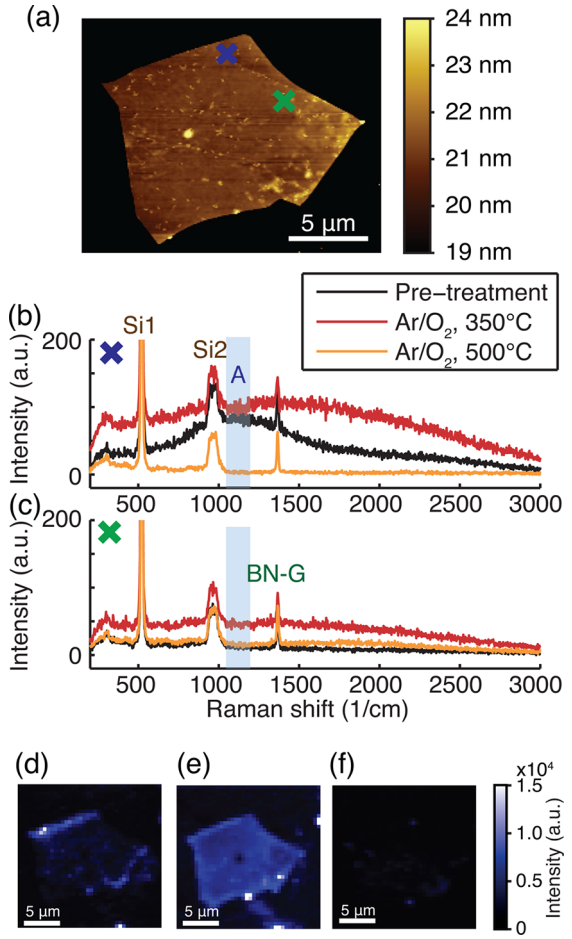

Figure 4. Effect of heat treatment in Ar/O_2 atmosphere in the presence of adhesive residue. (a) AFM topography of h-BN flake exfoliated on SiO_2 after annealing in Ar/O_2. During heat treatment, adhesive residue present on the flake forms prominent topographical features. The evolution of Raman spectra with heat treatment steps at 350 and 500 °C is shown for locations (b) where a significant amount of adhesive residue was initially present (blue cross), and (c) where no adhesive residue was visible before treatment (green cross). Spectral intensity maps obtained by integrating over a region that is dominated by the spectral response due to adhesive residue (region A, shaded in blue) are shown (d) before heat treatment, (e) after treatment in Ar/H_2 at 350 °C, (f) after treatment in Ar/H_2 at 500 °C.

The elimination of photoresist residue by the same procedure is shown in Figure 5. For a h-BN flake treated with photoresist as in standard lithographic processes, following treatment in Ar/O_2 at 500 °C, the AFM topography image (Figure 5a) exhibits few notable surface features. The evolution of Raman spectra is shown for positions where phoresist residue (Figure 5b), or both photoresist and adhesive residue (Figure 5c) were initially present. Treatment in Ar/O_2 at 350 °C modifies but does not remove the excess spectra, again reminiscent of spectra after treatment in Ar/H_2 atmosphere at this temperature. In contrast, treatment in Ar/O_2 at 500 °C completely removes the excess spectrum. The spectral maps shown in Figure 5d–f demonstrate that this result holds for almost any location on the h-BN flake.

On the basis of the similarities in the Raman spectra for h-BN flakes heat treated only up to 350 °C in either Ar/H_2 or Ar/O_2, it appears that the effects of this treatment are purely thermal and do not involve chemical reaction with the gases in the furnace. In contrast, at 500 °C the gaseous environment appears to be the relevant control parameter. Ar/H_2 heat treatment produces new Raman features associated with melted

dx.doi.org/10.1021/nl3011726 | *Nano Lett.* 2012, 12, 4449–4454

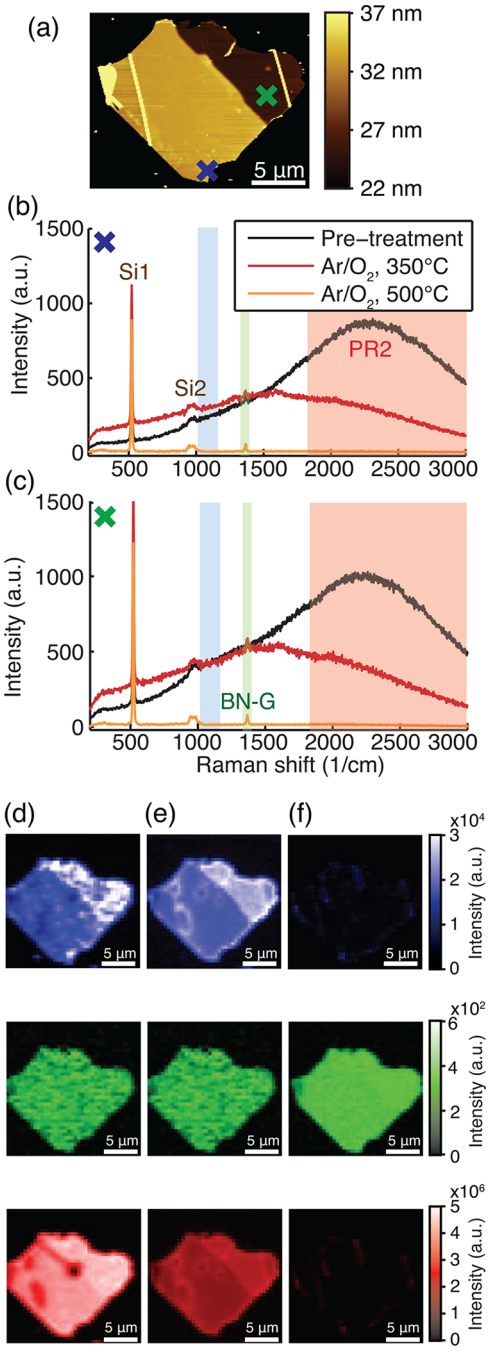

Figure 5. Effect of heat treatment in Ar/O_2 atmosphere in the presence of photoresist residue. (a) AFM topography of h-BN flakes on a SiO_2 substrate, after spin-coating with photoresist, resist removal with acetone and IPA, and subsequent heat treatment. (b,c) Raman spectra acquired at locations of different h-BN flake thickness: (b) 32 nm (blue cross) and (c) 25 nm (green cross). Almost all residue is eliminated with 500 °C treatment in Ar/O_2. Maps of the sample's Raman response (d) prior to heat treatment, (e) after treatment in Ar/H_2 at 350 °C, and (f) after subsequent heat treatment in Ar/H_2 at 500 °C are obtained by integrating over the spectral range dominated by the broad excess spectrum associated with photoresist residue (region PR2, shaded in red), and over the range occupied by the G-band of h-BN (shaded in green).

or burnt organic polymers, whereas Ar/O_2 treatment removes all spectra other than those of h-BN and the substrate.

We note that heat treatment at 500 °C in Ar/H_2 atmosphere appears to induce a redistribution of foreign material on h-BN, as seen in Figure 3d–f. Furthermore, the luminescence intensities suggest that a reconfiguration takes place in the organic adsorbates; regions that initially have a stronger photoresist signature (Figure 3d,e) show a weaker photoresist signature after the 500 °C treatment (Figure 3f), and vice versa. This intensity inversion in the photoresist luminescence signature coincides with the appearance of a D-band indicative of amorphous graphitized material, and spectral maps document a clear spatial correlation between features visible in the two bands. Since our focus is on the development of a recipe that eliminates organic adsorbates, we do not further investigate the origin of these phenomena induced by the conventional Ar/H_2 heat treatment.

It is interesting to note that the Raman signatures of adhesive and photoresist residues appear predominantly on the h-BN flakes and are absent on the SiO_2 substrate, both for unbaked samples and after heat treatment. This suggests that organic polymer residue attaches preferentially to the h-BN, or alternatively that the h-BN substrate leads to a luminescence enhancement of the adsorbed organic signal. Our AFM measurements indicate the presence of organic residue throughout the scanned areas, including the SiO_2 substrate, supporting the second hypothesis. It is not obvious that the broad luminescence peaks observed for unbaked samples and after conventional Ar/H_2 treatment stem from material adsorbed to the top surface of h-BN, as this luminescence could also be caused by an organic film trapped between SiO_2 and h-BN. Such contaminants would likely have less effect on graphene on top of the h-BN flake but could still cause hysteresis in backgating across the SiO_2 and h-BN.

By confocal Raman microscopy we test the impact of applying this same cleaning method directly to graphene sheets deposited on h-BN flakes, and we report preliminary electrical transport measurements. For sample preparation, we first clean an exfoliated h-BN flake in Ar/O_2 atmosphere at 500 °C, transfer graphene sheets onto the h-BN, and perform a second Ar/O_2 cleaning cycle on the assembled stack at 500 °C. Raman microscopy consistently indicates that the treatment described above results in graphene sheets of very high quality. Figure 6a shows representative Raman spectra of monolayer and bilayer graphene sheets on the h-BN flake. These Raman spectra are composed only of the known spectra of SiO_2, h-BN, and graphene, which provides evidence that the Ar/O_2 process successfully removed all organic contaminants. The high quality of both graphene sheets is reflected in the absence of a D-band (Figure 6b), suggesting that this second Ar/O_2 treatment at 500 °C does not damage graphene, and raising the possibility that our cleaning procedure can be applied on h-BN and graphene alike, facilitating the preparation of devices involving multiple layers, such as h-BN/(graphene/h-BN)$_x$.[14]

To test this idea, we perform additional processing to deposit contacts, and a third milder heat treatment in Ar/H_2 at 325 °C. (We found that to perform a third Ar/O_2 treatment step at the higher temperature, 500 °C, leads to contact degradation, rendering two-terminal resistances greater than 10 GΩ.) Our 2- and 3-terminal transport measurements[15] yield hole mobilities around 30,000 $cm^2/(V\,s)$ (room T) and 60,000 $cm^2/(V\,s)$ (4 K) for monolayer graphene in three separate samples. Electron mobilities are equal or lower by up to a factor of 2. These mobilities are achieved without any in situ current annealing, which is normally needed to achieve the highest mobilities for graphene on h-BN. The charge degeneracy point of several graphene sheets after this processing without any current annealing at room temperature is at backgate voltages between

dx.doi.org/10.1021/nl3011726 | Nano Lett. 2012, 12, 4449–4454

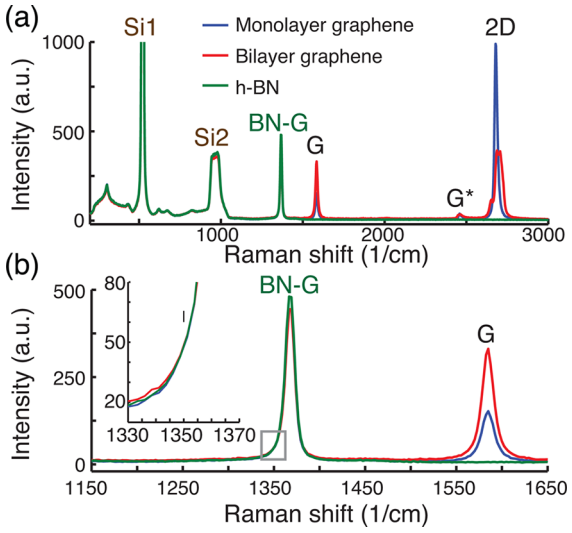

Figure 6. (a) Measured Raman spectra of monolayer (red line) and bilayer (blue line) graphene transferred onto a h-BN/SiO_2 substrate, and the spectrum of the h-BN/SiO_2 substrate alone (green line). This sample was heat treated in Ar/O_2 at 500 °C both before and after graphene transfer. The spectral components originate solely from the SiO_2 substrate, the h-BN flake, and the graphene sheets. (b) Magnified view of the h-BN and graphene G-bands. Inset: further magnification, focusing on the spectral range in the vicinity of ~1350 cm^{-1}, where a graphene D-band would be expected to be visible, overlapping with the flank of the h-BN G-peak. Within the precision of our measurement (<1% of graphene G-peak height. For comparison, the length of the black line shown in the inset at 1350 cm^{-1} corresponds to 2% of graphene G-peak height), spectra of graphene/h-BN and of h-BN alone coincide, indicating that graphene sheets have no pronounced D-band.

−1 and 0 V, indicating that graphene on h-BN substrates remains undoped upon exposure to air (1 V ≐ 7.17×10^{10} cm^{-2}), which is in contrast to typical results for graphene on SiO_2.

We now discuss in more detail methods used to fabricate and characterize samples discussed in this paper. Flakes of h-BN were produced by mechanical exfoliation of monocrystalline bulk h-BN[16] and deposited onto thermally oxidized silicon wafer pieces (t_{Ox} = 300 nm). For exfoliation, we used wafer-processing polymethyl acrylate-adhesive tape (Ultron Systems Inc., P/N: 1007R), keeping the substrate and tape at 50 °C for 4 min. Photoresist processing consisted of spin coating Shipley 1813 (propylene glycol monomethyl ether acetate 71−76%, mixed cresol novolak resin 10−20%, fluoroaliphatic polymer esters 0.01−1%, diazo photoactive compound 1−10%, cresol 0.01−0.99%) onto the chip at 5.5 krpm for 40 s, a 60 s hot plate bake at 90 °C, and subsequent resist removal by successively soaking in acetone and IPA. Heat treatment of samples was performed using a 1 in. quartz tube furnace. Gas pressure was kept at ambient, and gas flow rates were 500 sccm Ar and 500 sccm H_2 for the conventional treatment recipe; our alternative treatment was performed using 500 sccm Ar and 50 sccm O_2. Typically, heat treatment lasted 3−4 h. No differences due to variations in duration were discernible. On heating, the furnace was ramped to its target temperature at the rate of about 85 K/min. Cooling took place at a slower rate of approximately 10 K/min. AFM scans were performed on a Park XE-100 (Park Systems) in intermittent contact mode. A confocal scanning Raman microscope (WiTec alpha 500) was used to acquire Raman maps with an excitation wavelength of 532 nm, using a 50× objective, with a laser spot size ≈1 μm. Irradiation power at the sample was kept at ≈1 mW to avoid heating effects and sample damage with an integration time of 200 ms/pixel. The Raman spectra in Figure 6 were acquired with an integration time of 100 s per spectrum.

We create spatial maps of the h-BN flakes by integrating over specific regions of the Raman spectrum. Spectra presented in Figures 2−5 have consistent color-coding to mark these regions. The integration range 1350−1385 cm^{-1} (shaded in green) captures the G-band peak of h-BN centered at 1367 cm^{-1}.[17−19] Since this peak resides on a very large and broad background signal, integration is performed after subtraction of a linear background. Integration over the region 1475−1725 cm^{-1} (shaded in yellow) provides a measure for the graphitic G-band peak centered at 1600 cm^{-1} (see Figure 3b,c). This broad G-band, together with the associated broad D-band centered at 1350 cm^{-1}, are signatures of the formation of amorphous graphitic material from photoresist residue upon heating to 500 °C in Ar/H_2 atmosphere.[12,13] (Linear background subtration is performed prior to integration for this spectral range.) A luminescence signal specific to adhesive residue from the exfoliation process is centered around 1075 cm^{-1}. Integration of this peak is performed over the range 1050−1200 cm^{-1} (region A, shaded in blue). Finally, a luminescence signal specific to photoresist is centered around 2300 cm^{-1}. Integration of this peak is performed over the range 1800−3000 cm^{-1} (region PR2, shaded in red).

In conclusion, we have demonstrated a recipe for the successful removal of organic contaminants from mechanically exfoliated h-BN flakes on SiO_2, especially of contaminants arising from adhesive and from standard photolithographic processes. It will be interesting to further explore the effect of this recipe on mobility and other electronic properties of graphene subsequently deposited on the h-BN substrate.

■ ASSOCIATED CONTENT

Ⓢ Supporting Information

Details of the graphene transfer process and graphene transport measurements. This material is available free of charge via the Internet at http://pubs.acs.org.

■ AUTHOR INFORMATION

Corresponding Author

*E-mail: (A.G.F.G.) ag254@stanford.edu; (D.G.-G.) goldhaber-gordon@stanford.edu.

Notes

The authors declare no competing financial interest.

■ ACKNOWLEDGMENTS

The authors thank Julie Bert, Georgi Diankov, James Hone, Pablo Jarillo-Herrero, Markus König, and Javier Sanchez-Yamagishi for useful discussions. We acknowledge the support of the FENA Focus Center, one of six research centers funded under the Focus Center Research Program (FCRP), a Semiconductor Research Corporation entity. A.G.F.G. was also funded in part by the Center for Probing the Nanoscale, an NSF NSEC, supported under Grant PHY-0830228. M.N. was sponsored by the Office of Naval Research MURI on graphene, and J.R.W. was supported by a grant from the W. M. Keck Foundation.

■ REFERENCES

(1) Dean, C. R.; Young, A. F.; Meric, I.; Lee, C.; Wang, L.; Sorgenfrei, S.; Watanabe, K.; Taniguchi, T.; Kim, P.; Shepard, K. L.;

Hone, J. Boron nitride substrates for highquality graphene electronics. *Nat. Nanotechnol.* **2010**, *5*, 722−6.
(2) Wang, H.; Taychatanapat, T.; Hsu, A. BN/Graphene/BN Transistors for RF Applications. *Electron Device Lett.* **2011**, *32*, 1209−1211.
(3) Sanchez-Yamagishi, J.; Taychatanapat, T.; Watanabe, K.; Taniguchi, T.; Yacoby, A.; Jarillo-Herrero, P. Quantum Hall Effect, Screening, and Layer-Polarized Insulating States in Twisted Bilayer Graphene. *Phys. Rev. Lett.* **2012**, *108*, 1−5.
(4) Xue, J.; Sanchez-Yamagishi, J.; Bulmash, D.; Jacquod, P.; Deshpande, A.; Watanabe, K.; Taniguchi, T.; Jarillo-Herrero, P.; LeRoy, B. J. Scanning tunnelling microscopy and spectroscopy of ultra-flat graphene on hexagonal boron nitride. *Nat. Mater.* **2011**, *10*, 282−5.
(5) Decker, R.; Wang, Y.; Brar, V. W.; Regan, W.; Tsai, H.-Z.; Wu, Q.; Gannett, W.; Zettl, A.; Crommie, M. F. Local Electronic Properties of Graphene on a BN Substrate via Scanning Tunneling Microscopy. *Nano Lett.* **2011**, *11*, 2291−2295.
(6) Hwang, E.; Adam, S.; Sarma, S. Carrier Transport in Two-Dimensional Graphene Layers. *Phys. Rev. Lett.* **2007**, *98*, 2−5.
(7) Martin, J.; Akerman, N.; Ulbricht, G.; Lohmann, T.; Smet, J. H.; von Klitzing, K.; Yacoby, A. Observation of electron-hole puddles in graphene using a scanning singleelectron transistor. *Nat. Phys.* **2008**, *4*, 144−148.
(8) Katsnelson, M. I.; Geim, A. K. Electron scattering on microscopic corrugations in graphene. *Philos. Trans. R. Soc. London, Ser. A* **2008**, *366*, 195−204.
(9) Jung, S.; Rutter, G. M.; Klimov, N. N.; Newell, D. B.; Calizo, I.; Hight-Walker, A. R.; Zhitenev, N. B.; Stroscio, J. a. Evolution of microscopic localization in graphene in a magnetic field from scattering resonances to quantum dots. *Nat. Phys.* **2011**, *7*, 245−251.
(10) Feldman, B. E.; Martin, J.; Yacoby, A. Broken-symmetry states and divergent resistance in suspended bilayer graphene. *Nat. Phys.* **2009**, *5*, 889−893.
(11) Mysen, B.; Finger, L.; Virgo, D.; Seifert, F. Curve-fitting of Raman spectra of silicate glasses. *Am. Mineral.* **1982**, *67*, 686−695.
(12) Ferrari, A. C.; Robertson, J. Interpretation of Raman spectra of disordered and amorphous carbon. *Phys. Rev. B* **2000**, *61*, 95−107.
(13) Dumont, M.; Chollon, G.; Dourges, M.; Pailler, R. Chemical, microstructural and thermal analyses of a naphthalene-derived mesophase pitch. *Carbon* **2002**, *40*, 1475−1486.
(14) Britnell, L.; Gorbachev, R. V.; Jalil, R.; Belle, B. D.; Schedin, F.; Mishchenko, A.; Georgiou, T.; Katsnelson, M. I.; Eaves, L.; Morozov, S. V.; Peres, N. M. R.; Leist, J.; Geim, A. K.; Novoselov, K. S.; Ponomarenko, L. A. Field-effect tunneling transistor based on vertical graphene heterostructures. *Science* **2012**, *335*, 947−50.
(15) See Supporting Information for more details.
(16) Watanabe, K.; Taniguchi, T.; Kanda, H. Direct-bandgap properties and evidence for ultraviolet lasing of hexagonal boron nitride single crystal. *Nat. Mater.* **2004**, *3*, 404−9.
(17) Babich, I. Raman spectrum of hexagonal boron nitride. *Theor. Exp. Chem.* **1974**, *8*, 594−595.
(18) Arenal, R.; Ferrari, A. C.; Reich, S.; Wirtz, L.; Mevellec, J.-Y.; Lefrant, S.; Rubio, A.; Loiseau, A. Raman Spectroscopy of Single-Wall Boron Nitride Nanotubes. *Nano Lett.* **2006**, *6*, 1812−6.
(19) Gorbachev, R. V.; Riaz, I.; Nair, R. R.; Jalil, R.; Britnell, L.; Belle, B. D.; Hill, E. W.; Novoselov, K. S.; Watanabe, K.; Taniguchi, T.; Geim, A. K.; Blake, P. Hunting for monolayer boron nitride: optical and Raman signatures. *Small* **2011**, *7*, 465−8.